

Study of near-trapped modes and fictitious frequencies using null-field integral equation

Chine-Feng Wu^{1*}, Yi-Jhou Lin¹, I-Lin Chen², Jeng-Tzong Chen^{1,3}

¹Department of Harbor and River Engineering
National Taiwan Ocean University, Keelung, Taiwan

²Department of Naval Architecture
National Kaohsiung Marine University, Kaohsiung, Taiwan

³Department of Mechanical and Mechatronics Engineering
National Taiwan Ocean University, Keelung, Taiwan

*M97520023@mail.ntou.edu.tw

NSC PROJECT: NSC97-2221-E-019-015-MY3

ABSTRACT

In this paper, we employ the null-field integral equations to solve the scattering of water waves by bottom-mounted vertical circular cylinders. Based on the null-field integral equations in conjunction with degenerate kernels and Fourier series, we can avoid using principal-values sense in calculating singular integral, even though a null-field point is exactly located on the real boundary. This gain is owing to the introduction of degenerate kernels for fundamental solutions. Two kinds of peaks for the resultant force on the cylinder versus the wavenumber are observed. First, the critical (physical) wavenumber for the near-trapped mode is numerically detected. Second, the peak occurs at the fictitious frequency (mathematics) due to the integral formulation for exterior Helmholtz problems. Both peaks of near-trapped mode and fictitious frequency are physically and mathematically realizable, respectively. By increasing the number of Fourier terms, peaks due to fictitious frequencies are suppressed to be smooth while the peak value due to the near-trapped mode still keeps a sharp constant. Besides, the effect of angle of incident wave on the near-trapped mode is studied in this paper. Furthermore, a disorder of one cylinder by changing the radius and the position of center can suppress the occurrence of near-trapped mode due to the destruction of the periodical pattern. Numerical examples were demonstrated to show the validity of the present formulation.

Keywords: fictitious frequency, near-trapped modes, null-field integral equations, water wave, scattering problem.

1. INTRODUCTION

For designing the offshore platforms mounted on the sea bed, such as oil platforms which consist of a number of legs, it is important to understand the interaction between the vertical cylinders and plane wave. There is considerable interest for countries with long coasts, *e.g.*, USA, Japan and Taiwan. For the problem of plane waves impinging on vertical cylinders, a closed-form solution of force on a single vertical cylinder was derived by MacCamy and Fuchs [1]. The similar analysis extended to two cylinders was investigated by Spring and Monkmeyer [2]. They used the addition theorem to analytically derive the scattered-wave solution. Not only equal size but also unequal size of the cylinders subject to the incident wave of arbitrary angle was analyzed. They claimed that their method is a direct approach, since they formulated the problem by using a linear algebraic system and the solution is obtained easily from a single matrix inversion. A different method presented by Twersky [3] is called the multiple-scattering approach. In his approach, he took one cylinder at a time and scattering coefficient was solved sequentially. Besides, the boundary conditions which they solved are also different. Simon [4] as well as McIver and Evans [5] proposed an approximate solution based on the assumption that the cylinders are widely spaced. Later, Linton and Evans [6] also used the same approximate method which proposed earlier by Spring and Monkmeyer [2]. The main contribution was to provide a simple formula for the potential on the surfaces of the cylinders which makes the computation of forces much more straightforward. However, their results of four cylinders [6] were incorrect and corrigendum was given in Linton and Evans [7], Chen, Lee and Lin [8].

Trapped modes and near-trapped modes appear in different fields, such as string vibration, hydraulic engineering, earthquake engineering, ocean engineering and physics as described below in Figure 1. (1) String

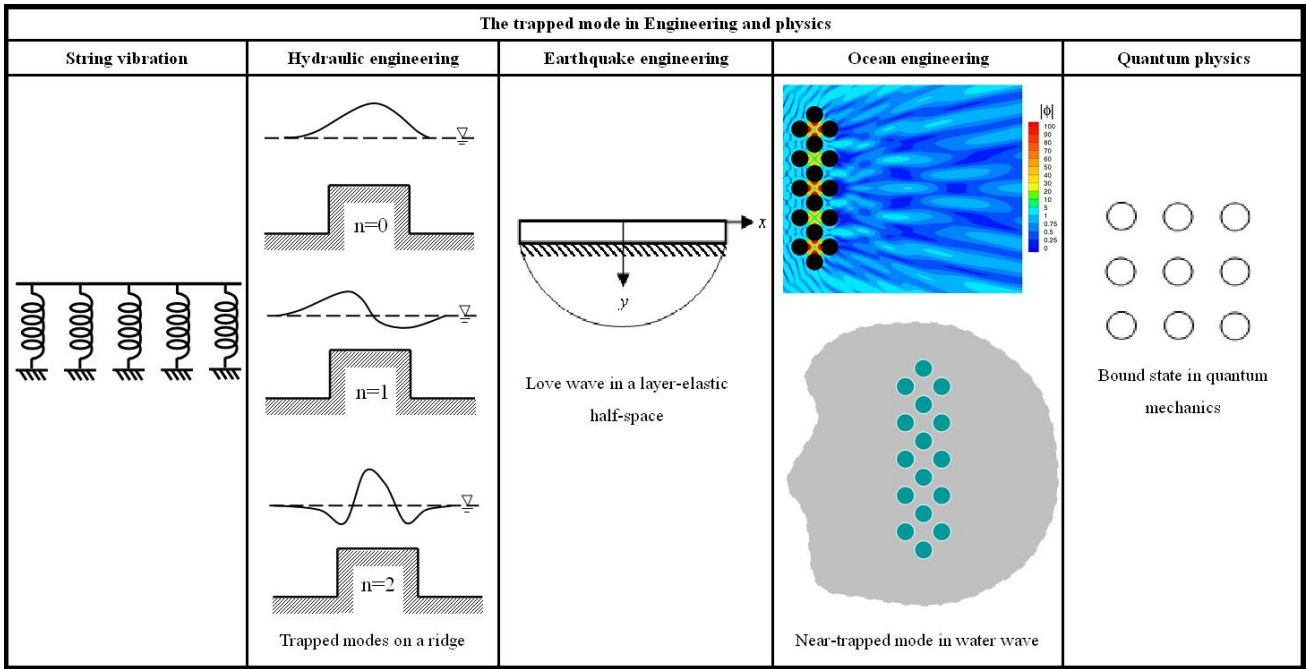


Figure 1 Near-trapped modes in physics and engineering

vibration : A string vibration can be modeled by a wave equation. When this system is subject to an incident wave, the spring may have a near-trapped mode under a certain spring layout and incident wave number. (2)

Hydraulic engineering : In hydraulic engineering, certain harmonic waves may exist at a depth discontinuity, but are unable to propagate from shallow to deep water [9, 10]. This phenomenon also belongs to one kind of near-trapped modes. (3)

Earthquake engineering : In earthquake engineering, surface wave may seriously result in damage for structures. For a thin-layer inclusion in a half-space medium, trapped wave may be present, e.g., Love wave [11] or Stonely wave. (4)

Ocean engineering : In ocean engineering, the construction of offshore platform is subjected to wave loads all the year. Duclos and Clément [12] and Williams and Li [13] proposed a simplified model of linear theory to simulate the interaction between cylinders subject to the incident wave. In this analysis, a specific distance between cylinders in companion with a certain wave number may cause a near-trapped mode. Discussions on this topic will be addressed in this paper. (5)

Quantum physics : The trapped mode, previously mentioned, occurs in physics as well as engineering. The bound state in a square-well potential in quantum mechanics is another case of trapped modes.

We will study the near-trapped mode by using null-field integral equation approach. The null-field integral equation approach was successfully employed to solve the scattering problems of water wave across an array of circular cylinders [8]. To fully utilize the geometry of circular boundary, not only Fourier series for boundary densities as previously used by many researchers but also the degenerate kernel for fundamental solutions in the present formulation are incorporated into the null-field integral equation. Several

advantages such as mesh-free generation, well-posed model, principal-value free, elimination of boundary-layer effect and exponential convergence, over the conventional boundary element method (BEM) are achieved. The near-trapped modes in physics were observed in a consistent way of other works [14]. However, the fictitious frequency in mathematics for the exterior Helmholtz problem when using BEM was not recorded in their paper.

For water wave problems, the existence of the irregular frequencies represents the most serious drawback of the boundary integral equation method, Ohmatsu [15] presented a combined integral equation method (CIEM) which was similar to the CHIEF-block method for acoustics proposed by Wu and Seybert [16]. Many researchers on exterior acoustics also encountered the problem of the fictitious frequency. To the authors' best knowledge, no paper simultaneously discussed the near-trapped mode in physics and fictitious frequency in mathematic. When near-trapped modes and fictitious frequencies both appear, how to recognize the source of nonuniqueness becomes an interesting and important issue.

Regarding the fictitious frequency, two ideas Burton-Miller (B&M) [17] approach and CHIEF [18] method, have been proposed to deal with this problem. The former one needs hypersingular formulation while the latter one may take risk once the CHIEF point falls in the node of corresponding interior modes. Dokumaci [19] and Juhl [20] both pointed out that numerical oscillation becomes serious as the number of boundary elements increases. On the other hand, Lee and Chen [21] found that the numerical instability can be suppressed by increasing the number of Fourier series terms by using null-field integral equations. A numerical example of a plate with two holes subject to an incident flexural wave demonstrated this point. We may wonder if it's possible

to suppress the occurrence of fictitious frequency free of B&M approach and CHIEF method for the water wave problem. The answer is positive in this paper.

In this paper, we focus on the null-field integral equations to solve the scattering of water waves. Both the near-trapped mode (nonuniqueness in physics) and the fictitious frequency (nonuniqueness in mathematics) are addressed and extracted out in this paper. In Section 2, we introduce the formulation of null-field integral equation for the Helmholtz problem. Some examples are demonstrated in Section 3 for the near-trapped mode by using our approach. Finally, we draw out some conclusion item by item in Section 4.

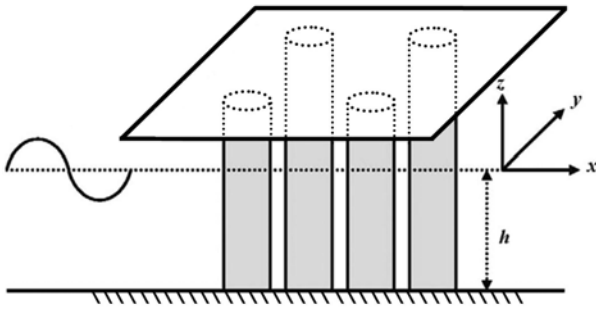


Figure 2 Problem statements of water waves with an array of vertical cylinders

2. PROBLEM STATEMENT AND INTEGRAL FORMULATION

2.1 Problem statement

Now we assume N vertical cylinders mounted at $z = -h$ upward to the free surface as shown in Figure 2. The water wave problem's governing equation is the Laplace equation

$$\nabla^2 \Phi(x, y, z, t) = 0, \quad (x, y, z) \in D, \quad (1)$$

where ∇^2 and D are the Laplacian operator and the domain of interest, respectively, and $\Phi(x, y, z, t)$ is the velocity potential, which satisfies the boundary conditions of seabed, kinematic boundary condition at free surface and dynamic boundary condition at free surface as shown below:

$$-\frac{\partial \Phi}{\partial n} = 0, \quad \text{at } z = -h(x, y), \quad (2)$$

$$-\Phi_z = H_t - \Phi_x H_x - \Phi_y H_y, \quad \text{at } z = H(x, y, t), \quad (3)$$

$$-\Phi_t + gz + \frac{1}{2}(\Phi_x^2 + \Phi_y^2 + \Phi_z^2) = B(t), \quad (4)$$

at $z = H(x, y, t)$,

where g is the gravity acceleration, $B(t)$ is the Bernoulli constant and $H(x, y, t)$ is the free-surface elevation. Based on the linear water wave theory, we can use the technique of separation variable for space and time,

$$\Phi(x, y, z, t) = \text{Re}\{\phi(x, y)f(z)e^{-i\omega t}\}, \quad (5)$$

where

$$f(z) = \frac{-igA \cosh(k(z+h))}{\omega \cosh(kh)}, \quad (6)$$

where k represents the wave-number, ω is the angular frequency and satisfies the dispersion relationship as follows:

$$k \tanh(kh) = \frac{\omega^2}{g}. \quad (7)$$

$H(x, y, t)$ can be defined by

$$H(x, y, t) = \text{Re}\{\eta(x, y)e^{-i\omega t}\}, \quad (8)$$

where

$$\eta(x, y) = A\phi(x, y), \quad (9)$$

and A represents the amplitude of incident wave of angle θ_{inc} as shown below:

$$\phi_i(x, y) = e^{ik(x \cos \theta_{inc} + y \sin \theta_{inc})} \equiv e^{ikr \cos(\theta - \theta_{inc})}. \quad (10)$$

Substituting Eq.(5) into Eq.(1), we have

$$(\nabla^2 + k^2)\phi(x, y) = 0, \quad (x, y) \in D. \quad (11)$$

Rigid cylinders yield the Neumann boundary conditions as shown below:

$$\frac{\partial \phi(x, y)}{\partial n} = 0, \quad (x, y) \in B. \quad (12)$$

The dynamic pressure can be obtained by

$$p = -\rho_0 \frac{\partial \Phi}{\partial t} = \rho_0 g A \frac{\cosh(k(z+h))}{\cosh(kh)} \phi(x, y) e^{-i\omega t}, \quad (13)$$

where ρ_0 denotes the density. The two components of the first-order force X^j on the j th cylinder are given by integrating the pressure over the circular boundary as shown below:

$$\{X^j\} = -\frac{\rho_0 g A a_j}{k} \cdot \tanh(kh) \cdot \int_0^{2\pi} \phi(x, y) \begin{Bmatrix} \cos \theta_j \\ \sin \theta_j \end{Bmatrix} d\theta_j, \quad (14)$$

where a_j denotes the radius of the j th cylinder.

2.2 Dual boundary integral equations — the conventional version

The integral equation for the domain point can be derived from the third Green's identity [22], we have

$$2\pi u(x) = \int_B T(s, x)u(s)dB(s) - \int_B U(s, x)t(s)dB(s), \quad x \in D, \quad (15)$$

$$2\pi t(x) = \int_B M(s, x)u(s)dB(s) - \int_B L(s, x)t(s)dB(s), \quad x \in D, \quad (16)$$

where s are the source points, $t = \frac{\partial u(s)}{\partial n_s}$ and $U(s, x)$

is the fundamental function which satisfies

$$(\nabla^2 + k^2)U(s, x) = 2\pi\delta(x-s), \quad (17)$$

where δ is the Dirac-delta function. The other kernel

functions $T(s, x)$, $L(s, x)$ and $M(s, x)$ are defined by

$$T(s, x) = \frac{\partial U(s, x)}{\partial n_s}, \quad (18)$$

$$L(s, x) = \frac{\partial U(s, x)}{\partial n_x}, \quad (19)$$

$$M(s, x) = \frac{\partial^2 U(s, x)}{\partial n_s \partial n_x}, \quad (20)$$

where n_x and n_s denote the unit outward normal vector at the field point and the source point, respectively. By moving the field point x to the boundary, the dual boundary integral equations for the boundary point can be obtained as follows:

$$\pi u(x) = C.P.V \int_B T(s, x)u(s)dB(s) - R.P.V \int_B U(s, x)t(s)dB(s), \quad x \in B, \quad (21)$$

$$\pi t(x) = H.P.V \int_B M(s, x)u(s)dB(s) - C.P.V \int_B L(s, x)t(s)dB(s), \quad x \in B, \quad (22)$$

where $R.P.V.$, $C.P.V.$ and $H.P.V.$ denote the Riemann principal value (Riemann sum), Cauchy principal value and Hadamard (or so-called Mangler) principal value, respectively. By collocating of the field point x on the complementary domain, we obtain the dual null-field boundary integral equations as shown below:

$$0 = \int_B T(s, x)u(s)dB(s) - \int_B U(s, x)t(s)dB(s), \quad x \in D^c, \quad (23)$$

$$0 = \int_B M(s, x)u(s)dB(s) - \int_B L(s, x)t(s)dB(s), \quad x \in D^c, \quad (24)$$

where D^c denote the complementary domain.

2.3 Dual null-field integral formulation — the present version

By introducing the degenerate kernels, the collocation point can be located on the real boundary free of facing principal value using bump contours. Therefore, the representations of integral equations including the boundary point for the interior problem can be written as

$$2\pi u(x) = \int_B T^I(s, x)u(s)dB(s) - \int_B U^I(s, x)t(s)dB(s), \quad x \in D \cup B, \quad (25)$$

$$2\pi t(x) = \int_B M^I(s, x)u(s)dB(s) - \int_B L^I(s, x)t(s)dB(s), \quad x \in D \cup B, \quad (26)$$

and

$$0 = \int_B T^E(s, x)u(s)dB(s) - \int_B U^E(s, x)t(s)dB(s), \quad x \in D^c \cup B, \quad (27)$$

$$0 = \int_B M^E(s, x)u(s)dB(s) - \int_B L^E(s, x)t(s)dB(s), \quad x \in D^c \cup B, \quad (28)$$

once the kernels are expressed in term of an appropriate degenerate forms (denoted by superscript I and E) instead of the closed-form fundamental solution without distinction. It is noted that x in Eqs.(25)-(28) can exactly be located on the real boundary. For the exterior problem, the domain of interest is in the external region of the circular boundary and the complementary domain is in the internal region of the circle. Therefore, the null-field integral equations are represented as

$$2\pi u(x) = \int_B T^E(s, x)u(s)dB(s) - \int_B U^E(s, x)t(s)dB(s), \quad x \in D \cup B, \quad (29)$$

$$2\pi t(x) = \int_B M^E(s, x)u(s)dB(s) - \int_B L^E(s, x)t(s)dB(s), \quad x \in D \cup B, \quad (30)$$

and

$$0 = \int_B T^I(s, x)u(s)dB(s) - \int_B U^I(s, x)t(s)dB(s), \quad x \in D^c \cup B, \quad (31)$$

$$0 = \int_B M^I(s, x)u(s)dB(s) - \int_B L^I(s, x)t(s)dB(s), \quad x \in D^c \cup B. \quad (32)$$

Also, the collocation point, x , in Eqs.(29)-(32) can be exactly located on the real boundary. For various problems (interior or exterior), we use different kernel functions (denoted by superscripts “ I ” and “ E ”) so that the jump behavior across the boundary can be captured. Therefore, different expressions of the kernels for the interior and exterior observer points are used and they will be elaborated on latter.

2.4 Expansions of fundamental solution and boundary density

Based on the separable property, the kernel function $U(s, x)$ can be expanded into degenerate form by separating the source points and field points in the polar coordinates. Since degenerate kernels can describe the fundamental solutions in two regions (interior and exterior domains), the boundary integral equation (BIE) for the domain point of Eqs.(25)-(26) and Eqs.(29)-(30) and null-field BIE of Eqs.(27)-(28) and Eqs.(31)-(32) can be directly employed for the boundary point. In the real implementation, the null-field point can be exactly pushed on the real boundary since we introduce the expression of degenerate kernel for fundamental solutions. By using the polar coordinates, we can express $x = (\rho, \phi)$ and $s = (R, \theta)$. The four kernels U , T , L and M can be expressed in terms of degenerate kernels as shown below [23]:

$$U(s, x) = \begin{cases} U^I(R, \theta; \rho, \phi) \\ = \frac{-\pi i}{2} \sum_{m=0}^{\infty} \varepsilon_m J_m(k\rho) H_m^{(1)}(kR) \cos(m(\theta - \phi)), R \geq \rho, \\ U^E(R, \theta; \rho, \phi) \\ = \frac{-\pi i}{2} \sum_{m=0}^{\infty} \varepsilon_m H_m^{(1)}(k\rho) J_m(kR) \cos(m(\theta - \phi)), R < \rho, \end{cases} \quad (33)$$

$$T(s,x) = \begin{cases} T^I(R,\theta;\rho,\phi) \\ = \frac{-\pi ki}{2} \sum_{m=0}^{\infty} \varepsilon_m J_m(k\rho) H_m^{(1)}(kR) \cos(m(\theta-\phi)), R > \rho, \\ T^E(R,\theta;\rho,\phi) \\ = \frac{-\pi ki}{2} \sum_{m=0}^{\infty} \varepsilon_m H_m^{(1)}(k\rho) J_m'(kR) \cos(m(\theta-\phi)), R < \rho, \end{cases} \quad (34)$$

$$L(s,x) = \begin{cases} L^I(R,\theta;\rho,\phi) \\ = \frac{-\pi ki}{2} \sum_{m=0}^{\infty} \varepsilon_m J_m'(k\rho) H_m^{(1)}(kR) \cos(m(\theta-\phi)), R > \rho, \\ L^E(R,\theta;\rho,\phi) \\ = \frac{-\pi ki}{2} \sum_{m=0}^{\infty} \varepsilon_m H_m^{(1)}(k\rho) J_m(kR) \cos(m(\theta-\phi)), R < \rho, \end{cases} \quad (35)$$

$$M(s,x) = \begin{cases} M^I(R,\theta;\rho,\phi) \\ = \frac{-\pi k^2 i}{2} \sum_{m=0}^{\infty} \varepsilon_m J_m'(k\rho) H_m^{(1)}(kR) \cos(m(\theta-\phi)), R \geq \rho, \\ M^E(R,\theta;\rho,\phi) \\ = \frac{-\pi k^2 i}{2} \sum_{m=0}^{\infty} \varepsilon_m H_m^{(1)}(k\rho) J_m'(kR) \cos(m(\theta-\phi)), R < \rho, \end{cases} \quad (36)$$

where ε_m is the Neumann factor

$$\varepsilon_m = \begin{cases} 1, & m = 0, \\ 2, & m = 1, 2, \dots, \infty. \end{cases} \quad (37)$$

Equations (33)-(36) can be seen as the subtraction theorem instead of the addition theorem since we care $|x-s|$ not $|x+s|$. Mathematically speaking, the expressions of fundamental solutions in Eqs.(33)-(36) are termed degenerate kernels (or separable kernels) which can expand the kernel to sums of products of function of the field point x alone and functions of the source point s alone. If the finite sum of series is considered, the kernel is finite rank. As we shall see in the later sections, the theory of boundary integral equations with degenerate kernel is nothing more than the linear algebra. Since the potentials resulted from $T(s,x)$ and $L(s,x)$ are discontinuous across the boundary, the potentials of $T(s,x)$ and $L(s,x)$ for $R \rightarrow \rho^+$ and $R \rightarrow \rho^-$ are different. This is the reason why $R = \rho$ is not included in the expression for the degenerate kernels of $T(s,x)$ and $L(s,x)$ in Eqs.(34) and (35). The degenerate kernels simply serve as the means to evaluate regular integrals analytically and take the limits analytically. The reason is

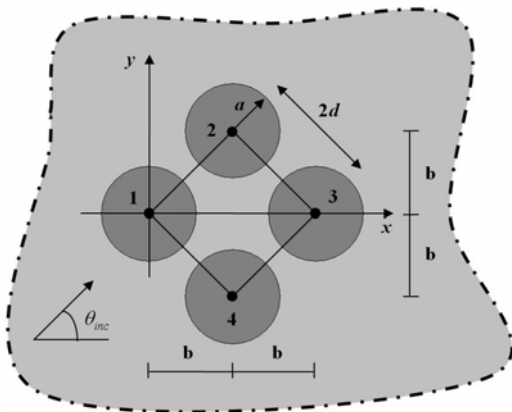


Figure 3 Sketch of four cylinders

that integral equation for the domain point of Eq.(25) and null-field integral equation of Eq.(27) yield the same algebraic equation when the limit is taken from the inside or from the outside of the region. Both limits represent the same algebraic equation that is an approximate counterpart of the boundary integral equation, that for the case of a smooth boundary has in the left-hand side term $\pi u(x)$ or $\pi t(x)$ rather than $2\pi u(x)$ or $2\pi t(x)$ for the domain point or 0 for the point outside the domain. Besides, the limiting case to the boundary is also addressed. The continuous and jump behavior across the boundary is well captured by the Wronskian property of Bessel function J_m and Y_m bases

$$\begin{aligned} W(J_m(kR), Y_m(kR)) \\ = Y_m'(kR) J_m(kR) - Y_m(kR) J_m'(kR) = \frac{2}{\pi kR}, \end{aligned} \quad (38)$$

as shown below

$$\begin{aligned} \int_0^{2\pi} (T^I(s,x) - T^E(s,x)) \cos(m\theta) R d\theta \\ = 2\pi \cos(m\phi), \quad x \in B, \end{aligned} \quad (39)$$

$$\begin{aligned} \int_0^{2\pi} (T^I(s,x) - T^E(s,x)) \sin(m\theta) R d\theta \\ = 2\pi \sin(m\phi), \quad x \in B. \end{aligned} \quad (40)$$

After employing Eqs.(39) and (40), Eq.(29) and Eq.(31) yield the same linear algebraic equation when x is exactly pushed on the boundary from the domain or the complementing domain.

In order to fully utilize the geometry of circular boundary, the boundary density $u(s)$ and its normal flux $t(s)$ can be approximated by employing the Fourier series. Therefore, we obtain

$$u(s) = a_0 + \sum_{n=1}^{\infty} (a_n \cos n\theta + b_n \sin n\theta), \quad (41)$$

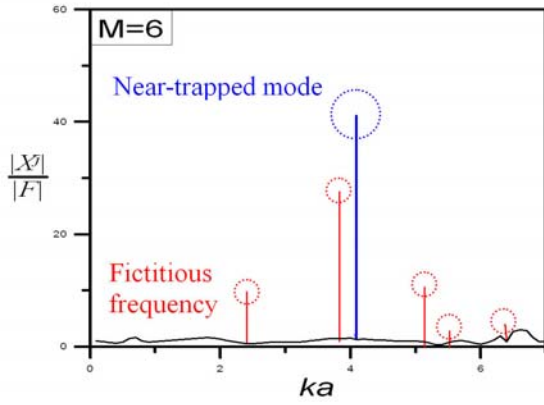
$$t(s) = p_0 + \sum_{n=1}^{\infty} (p_n \cos n\theta + q_n \sin n\theta), \quad (42)$$

where a_0, a_n, b_n, p_0, p_n and q_n are the Fourier coefficients and θ is the polar angle which is equally discretized. Equations (31) and (32) can be easily calculated by employing the orthogonal property of Fourier series. In the real computation, only the finite P terms are used in the summation of Eqs.(41) and (42).

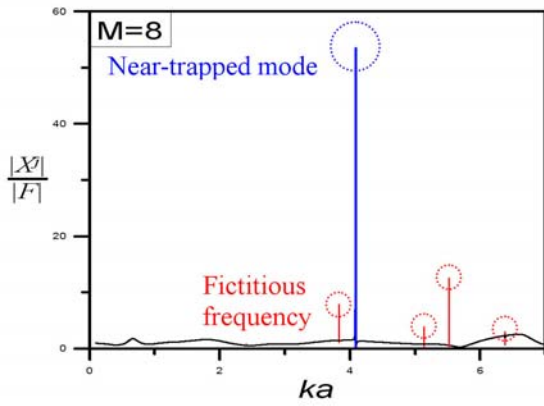
3. ILLUSTRATIVE EXAMPLES

Case 1: Near-trapped mode and fictitious frequency

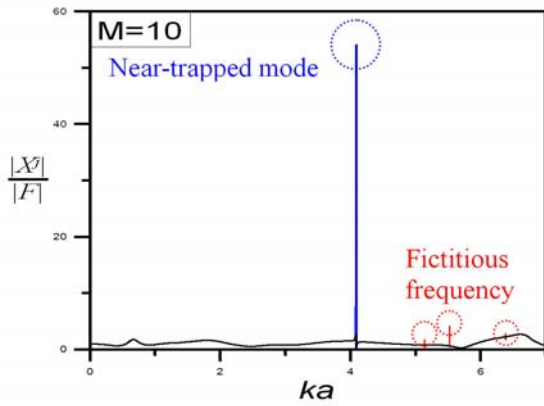
We consider the water wave problem by an array of four bottom-mounted vertical rigid circular cylinders with the same radius a located at the vertices of a square $(0, 0), (b, b), (2b, 0), (b, -b)$, as shown in Figure 3. Figures 4(a) to 4(e) show the forces in the direction of incident wave versus the wavenumber by using different number of Fourier terms. It's interesting to find that two kinds of peak occur. One kind of peak appears at the corresponding wavenumber which happens to be the zeros of Bessel function $J_n(kr)$, e.g., 2.4042 ($J_{0,1}$),



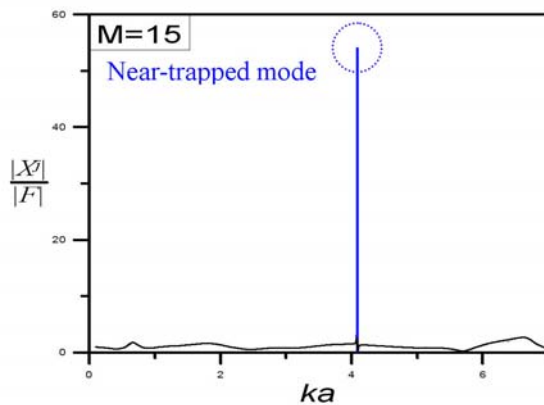
(a) M=6



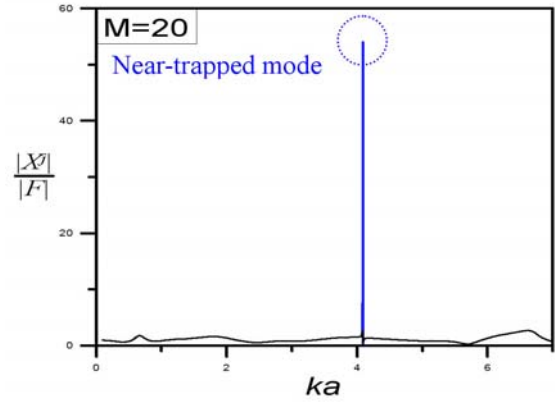
(b) M=8



(c) M=10



(d) M=15



(e) M=20

Figure 4 Resultant force on four cylinders against wavenumber, ka , (a) $M=6$, (b) $M=8$, (c) $M=10$, (d) $M=15$, (e) $M=20$ ($\theta_{inc} = 0^\circ$ and $a/d=0.8$)

3.8317 ($J_{1,1}$), 5.1356 ($J_{2,1}$), 5.5201 ($J_{0,2}$) and 6.3802 ($J_{3,1}$), etc.... The other peak occurs at the wavenumber of $k=4.08482$ which is physically-realizable as a near-trapped mode. Figure 4(e) shows that the peak due to fictitious (irregular) frequency is suppressed to be smooth after increasing the number of Fourier terms to be $M=20$, while the peak value due to the near-trapped mode still exists there even when the wavenumber of Fourier terms, M , increases. It's explained that fictitious frequencies occur when we employ BIEM to solve exterior Helmholtz problems. It belongs to numerical resonance instead of physical phenomenon. The peak value due to the near-trapped mode (physics) and fictitious frequency (mathematics) are both observed in the present paper since BIEM was utilized. Fictitious frequency is not present in the work of Evans and Porter [14] since they employed the Twersky's method.

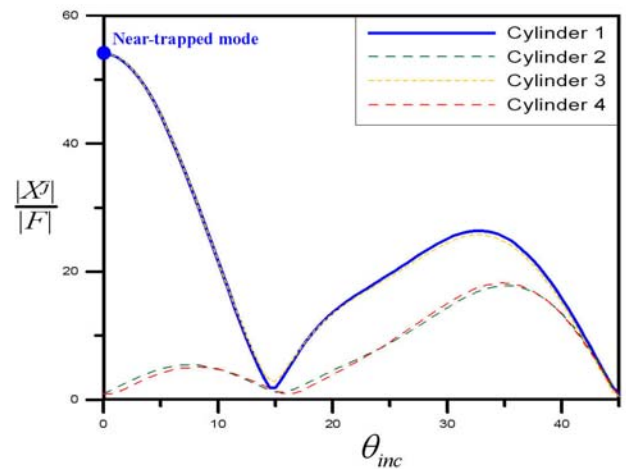


Figure 5 Effect of incident angle on the near-trapped mode.

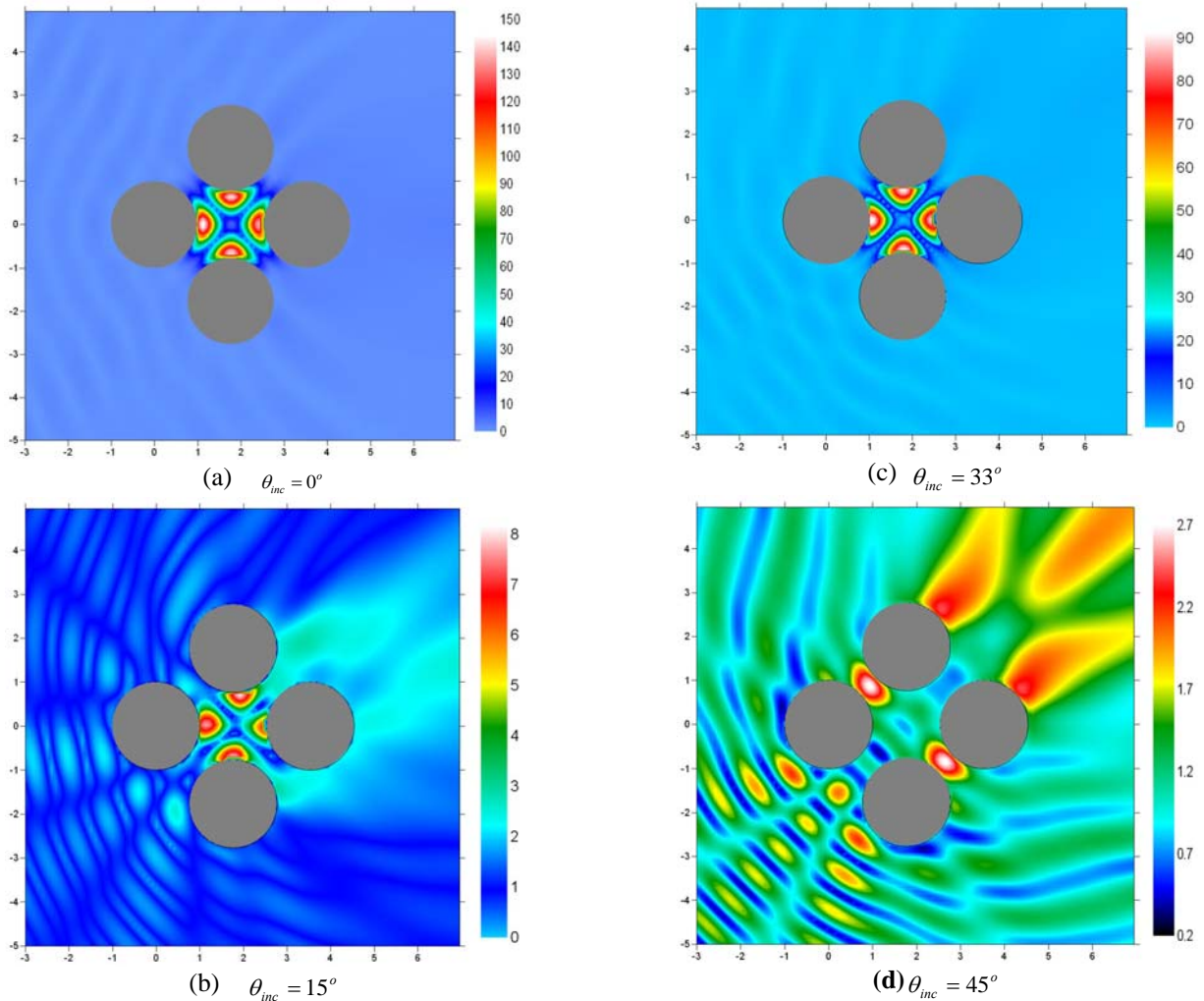


Figure 6 Near-trapped mode for the four cylinders at $ka=4.08482$, $a/d=0.8$. (a) $\theta_{inc} = 0^\circ$, (b) $\theta_{inc} = 15^\circ$, (c) $\theta_{inc} = 33^\circ$, (d) $\theta_{inc} = 45^\circ$

Case 2: Effect of incident angle on the near-trapped mode

Here, we consider the same problem of case 1 but focus on the effect of incident angle of wave on the near-trapped mode. Figure 5 shows the force versus the incident angle in the range of $\theta_{inc} = 0^\circ \sim 45^\circ$ for the case of $k=4.08482$ and $a/d=0.8$. Figures 6(a) - 6(d) show the contour of free-surface elevation by using different incident angles, (a) $\theta_{inc} = 0^\circ$, (b) $\theta_{inc} = 15^\circ$, (c) $\theta_{inc} = 33^\circ$ and (d) $\theta_{inc} = 45^\circ$, respectively. As predicted by [14], we reconfirm that over 150 times of the amplitude of incident wave and 54 times of the force over one single cylinder are verified for the case of $\theta_{inc} = 0^\circ$ by using our approach.

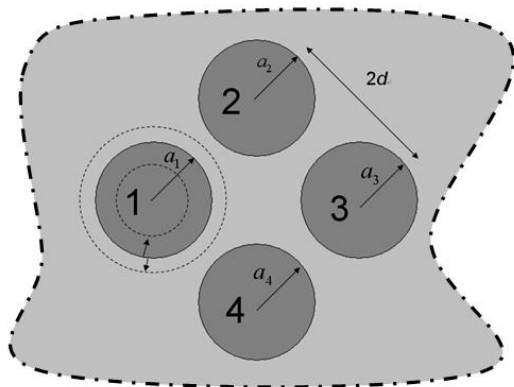
Case 3: Disorder of the periodical pattern

For the third case, the same condition of case 1 is considered except for the disorder of the cylinder 1. Two kinds of disorder are implemented. One is to perturb the radius of a cylinder to be different with other cylinders as shown in Figure 7(a). The other is to disturb the center of

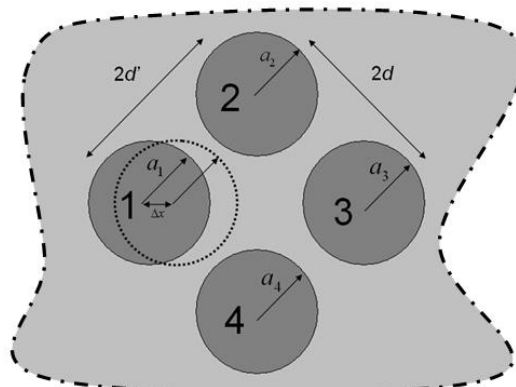
one cylinder as shown in Figure 7(b). After comparing with the result of [14], good agreement is made as shown Figures 8(a) and 8(b). The parameter study for the disorder on the near-trapped mode of $ka=4.08482$ is examined. Tables 1 and 2 indicate that the peak value for the near-trapped mode is reduced significantly due to the perturbation of radius and displacement of the center of one cylinder, respectively.

4. CONCLUSIONS

In this paper, we applied a null-field BIEM formulation by using degenerate kernels for water wave scattering problems with four circular cylinders. Discussions on the physical phenomena of near-trapped mode as well as the numerical phenomena due to fictitious frequency in BIEM were both addressed. The fictitious frequency is present and can be suppressed to be smooth in sacrifice of higher number of Fourier terms. In the meanwhile, the peak due to the near-trapped mode also occurs and its value keeps a constant. In the periodical array of four rigid circular cylinders, the effect of angle of incident wave on the near-trapped mode variation was examined. By perturbing the radius of one



(a) Perturbation of the radius for cylinder 1



(b) Disturbance of the center of cylinder 1

Figure 7 Sketch of four cylinders

cylinder ($a_1/d \neq 0.8$) or moving the center of one cylinder to destroy the periodical setup, the trapped mode was obviously suppressed. The free-surface elevation and resultant forces on each cylinder have been presented to illustrate the effect of angle of incident wave and disorder of the periodical layout on the near trapped modes. The results were compared well with those of Evans and Porter.

5. ACKNOWLEDGEMENT

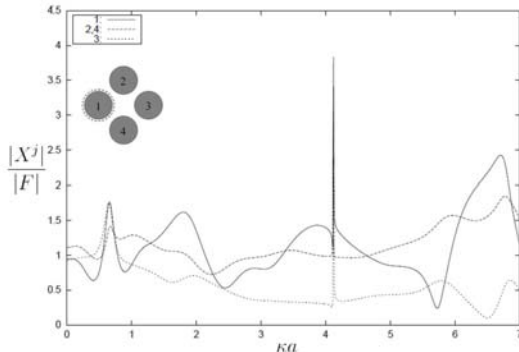
This research was partially supported by the National SCIENCE Council of Taiwan under Grant NSC 97-2221-E-019-015-MY3 for National Taiwan Ocean University.

6. REFERENCES

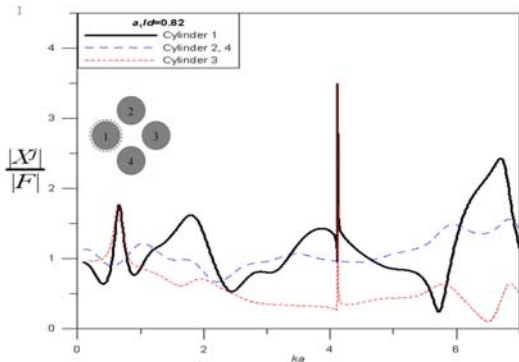
- [1] R.C. MacCamy and R.A. Fuchs, *Wave force on piles: A diffraction theory*, U. S. Army, Coastal Engineering Research Center, Technical Memorandum. Washington, D.C; 1954.
- [2] B.H. Spring and P.L. Monkmeyer, Interaction of plane waves with vertical cylinders, *Proceeding 14th International Conference on Coastal Engineering*, pp. 1828-1845, 1974.
- [3] V. Twersky, "Multiple scattering of radiation by an arbitrary configuration of parallel cylinders," *J. Acoust. Soc. Am.*, vol. 24, no. 1, pp.42-46, 1952.
- [4] M. J. Simon, "Multiple scattering in arrays of axisymmetric wave-energy devices," *J. Fluid Mech.*, vol.120, pp. 1-25, 1982.
- [5] P. McIver and D.V. Evans, "Approximation of wave forces on cylinder arrays," *Appl. Ocean Res.*, vol. 6, no. 2, pp. 101-107, 1984.
- [6] C.M. Linton and D.V. Evans, "The interaction of waves with arrays of vertical circular cylinders," *J. Fluid Mech.*, vol. 215, pp. 549-569, 1990.
- [7] C.M. Linton and D.V. Evans, "Corrigendum: The interaction of waves with arrays of vertical circular cylinders," *J. Fluid Mech.*, vol. 218, pp. 663, 1990.
- [8] J.T. Chen, Y.T. Lee and Y.J. Lin, "Interaction of water waves with arbitrary vertical cylinders using null-field integral equations," *Appl. Ocean Res.*, in press.
- [9] M.S. Longuet-higgins, "On the trapping of wave energy round islands," *J. Fluid Mech.*, vol. 29, pp. 781-821, 1967.
- [10] F.E. Snodgrass, W.H. Mund and G.R. Miller, "Long period waves over California's continental borderland, part I. background spectra," *J. Mar. Res.*, vol. 20, pp. 3-30, 1962.
- [11] A.E.H. Love, *Some Problems of Geodynamics*, Cambridge University Press; 1966.
- [12] G. Duclos and A.H. Clément, "Wave propagation through arrays of unevenly spaced vertical piles," *Ocean Eng.*, vol. 31, pp. 1655-1668, 2004.
- [13] A.N. Williams and W. Li, "Water wave interaction with an array of bottom-mounted surface-piercing porous cylinders," *Ocean Eng.*, vol. 27, pp. 841-866, 2000.
- [14] D.V. Evans and R. Porter, "Trapping and near-trapping by arrays of cylinders in waves," *J. Eng. Mathe.*, vol. 35, pp.149-179, 1999.
- [15] S. Ohmatsu, "A new simple method to eliminate the irregular frequencies in the theory of water wave radiation problems," *Papers of Ship Research Institute*, 1983.
- [16] T.W. Wu and A.F. Seybert, "A weighted residual formulation for the CHIEF method in acoustics," *J. Acoust. Soc. Am.*, vol. 90, no. 3, pp. 1608-1614, 1991.
- [17] A.J. Burton and G.F. Miller, "The application of integral equation methods to numerical solution of some exterior boundary value problems," *Proc. R. Soc. Lond., Ser. A, Math. phys. sci.*, vol. 323, pp. 201-210, 1971.
- [18] H.A. Schenck, "Improved integral formulation for acoustic radiation problem," *J. Acoust. Soc. Amer.*, vol. 44, pp. 41-58, 1968.
- [19] E. Dokumaci, "A study of the failure of numerical solutions in boundary element analysis of acoustic radiation problems," *J. Sound Vib.*, vol. 139, no. 1, pp. 83-97, 1990.
- [20] P. Juhl, "A numerical investigation of standard condenser microphones," *J. Sound Vib.*, vol. 177, no. 4, pp.433-446, 1994.
- [21] W.M. Lee and J.T. Chen, "Scattering of flexural wave in thin plate with multiple holes by using the

null-field integral equation approach,” *CMES*, vol. 37, no. 3, pp. 243-273, 2008.

- [22] J.T. Chen, H.K. Hong, “Review of dual boundary element methods with emphasis on hypersingular integrals and divergent series,” *Appl. Mech. Rev.*, vol. 52, pp.17-33, 1999.
- [23] J.T. Chen, K.H. Chen, I.L. Chen and L.W. Liu, “A new concept of modal participation factor for numerical instability in the dual BEM for exterior acoustics,” *Mech. Res. Commun.*, vol. 26, no. 2, pp. 161-174, 2003.



(a) Evans and Porter [14]



(b) Present method (M=20)

Figure 8 Resultant force on un-symmetric pattern of four cylinders against the wavenumber, ka , ($\theta_{inc} = 0^\circ$, $a_1/d = 0.82$, $a_i/d = 0.8, i=2,3,4$)

(a) Evans and Porter [14], (b) Present method

Table 1 Resultant force by changing radius to destroy the periodical setup. ($ka=4.08482$)

a_1/d	a_i/d $i=2,3,4$	Cylinder 1	Cylinder 3
		$\frac{ X^1 }{ F }$	$\frac{ X^3 }{ F }$
0.86	0.8	1.15	0.25
0.84	0.8	1.20	0.25
0.82	0.8	1.30	0.27
0.80	0.8	54.1	54.1
0.78	0.8	1.02	0.34
0.76	0.8	1.13	0.30
0.74	0.8	1.19	0.30

Table 2 Resultant force by moving the center of one cylinder to destroy the periodical setup. ($ka=4.08482$)

a_1/d'	a_i/d $i=2,3,4$	Cylinder 1	Cylinder 3
		$\frac{ X^1 }{ F }$	$\frac{ X^3 }{ F }$
0.86	0.8	1.15	0.29
0.84	0.8	1.20	0.28
0.82	0.8	1.27	0.27
0.80	0.8	54.1	54.1
0.78	0.8	1.12	0.27
0.76	0.8	1.17	0.26
0.74	0.8	1.16	0.26

零場積分方程於近陷阱模態與虛擬頻率之研究

吳建鋒^{1*}, 林羿州¹, 陳義麟², 陳正宗^{1,3}

¹ 國立台灣海洋大學河海工程學系

² 國立高雄海洋科技大學造船工程學系

³ 國立台灣海洋大學機械與機電工程學系

*M97520023@mail.ntou.edu.tw

**NSC PROJECT:
NSC97-2221-E-019-015-MY3**

摘要

本文採用零場積分方程求解多圓柱水波散射問題。透過零場積分方程並配合退化核與傅立葉級數，可將零場點直接放置到真實邊界上，並能免除以主值觀念計算奇異積分的困擾。文中在計算圓柱所受之合力對波數作圖時，觀察到兩種尖峰值現象。一個是數值實驗觀察到陷阱模態(物理上的)之臨界波數。另一個是以積分方程求解外域 Helmholtz 方程時，所出現的虛擬頻率(數學上的)。上述之陷阱模態和虛擬頻率之尖峰分別可用物理與數學觀點加以解釋。本文藉由增加傅立葉級數之項數，發現陷阱模態尖峰值仍保持不變，而虛擬頻率所引起的尖峰值則受抑制而趨於平滑。文中亦探討入射波之入射角度改變，對於陷阱模態所造成影響。此外，透過改變圓柱半徑或中心位置，來破壞圓柱週期性配置，證實可抑制陷阱模態的發生。最後本文用數值算例來證實本文方法之有效性。

關鍵詞： 虛擬頻率、近陷阱模態、零場積分方程、水波、散射問題。